Bull Volcanol (1995) 57:403–421

ORIGINAL PAPER

S. M. Straub

Contrasting compositions of Mariana Trough fallout tephra and Mariana Island arc volcanics: a fractional crystallization link

Received: January 12, 1995 / Accepted: August 10, 1995

Abstract Discrete Quaternary (<400 ka) tephra fallout layers (mostly <1 cm thick) within the siliceous oozes of the central Mariana Trough at 18°N are characterized by medium-K to high-K subalkalic volcanic glasses ($K_2O = 0.8$–3.2 wt.%) with high large-ion lithophile elements (LILE)/high-field-strength elements (HFSE) ratios and Nb depletion (Ba/La ≈ 35; Ba/Zr ≈ 3.5; La/Nb ≈ 4) typical for convergent margin volcanic rocks. Compositional zoning within layers ranges from basaltic to dacitic ($SiO_2 = 48$–71 wt.%; MgO = 0.7–6.5 wt.%); all layers contain basaltic andesites. The tephra layers are interpreted as single explosive eruptive events tapping chemically zoned reservoirs, the sources being the Mariana arc volcanoes (MAV) due to their proximity (100–400 km) and similar element ratios (MAV: Ba/La = 36 ± 7; Ba/Zr = 3.5 ± 0.9). The glasses investigated, however, contrast with the contemporaneous basaltic to dacitic lavas of the MAV by being more enriched in TiO_2 (≈1.2 wt.%; MAV ≈ 0.8 wt.%), FeO* (≈10 wt.%, MAV ≈ 8–9 wt.%), K_2O (≈1.1 wt.%; MAV ≈ 0.8 wt.%) and P_2O_5 (≈0.4 wt.%; MAV ≈ 0.2 wt.%). (Semi-)Incompatible trace elements (including Rare Earth Elements (REE)) of the *basaltic-andesitic and dacitic* glasses match those of the *dacitic* MAV lavas, which became enriched by fractional crystallization. Moreover, the glasses follow a tholeiitic trend of fractionation in contrast to MAV transitional trends and have a characteristic P_2O_5 trend that reaches a maximum of 0.6 wt.% P_2O_5 at ≈57 wt.% SiO_2, whereas MAV lavas increase linearly in P_2O_5 from 0.1 to 0.3 wt.% with increasing silica. Both explosive and effusive series are interpreted to have evolved in common magma reservoirs by convective fractionation. Similar parental magmas are suggested to have separated into coexisting Si-andesitic to dacitic and basaltic melts by in situ crystallization. The differentiated melt is interstitial in an apatite-saturated crystalline mush of plag + px ± ox ± ol at the cooler chamber margins in contrast to the less differentiated basaltic to basaltic–andesitic magmas, which are not yet saturated in apatite and occupy the chamber interior. Reinjection of interstitial melt into the chamber interior and mixing with larger melt fractions of the interior liquid (mixing ratios about ≈1:8–9) can explain the paradoxical behavior of apatite-controlled P and MREE variation in the basaltic andesite glasses and their MAV dacite-like fractionation patterns. The process may also account for the exclusively tholeiitic trend of fractionation of the glass shard series, but in situ crystallization alone cannot cause their absolute enrichment in (semi-)incompatible elements. The newly mixed melt is suggested to form the basaltic end member of the glass shard series. However, it must have become physically separated from the main MAV magma body (possibly by density-driven convective fractionation) in order to allow for further evolution of the contrasting geochemical paths as well as differentiation.

Key words Mariana volcanic arc · Submarine fallout tephra · Fractional crystallization

Editorial responsibility: S. Carey

S. M. Straub
Department of Volcanology and Petrology,
GEOMAR Research Center,
Wischhofstrasse 1–3, D-24148 Kiel, Germany
Tel.: 914-365-8662 (USA). Fax: 914-365-8155 (USA)
E-mail: smstraub@ldeo.columbia.edu

Present address: Lamont Doherty Earth Observatory of Columbia University, Palisades, New York 10964, USA

Introduction

Fallout tephra layers in marine sediments provide a high-resolution and temporally precise record of volcanic activity (e.g. Paterne et al. 1988; Arculus and Bloomfield 1992; Bednarz and Schmincke 1994). Submarine tephra studies have become increasingly important in the course of the DSDP/ODP drilling programs, because distal tephra deposits are often the only tool

for reconstructing the petrogenetic evolution of volcanic terrains, which are either buried under younger series or have been eroded (e.g. Hiscott and Gill 1992; Simon-Neuser and Schmincke in press).

The deposition of submarine fallout tephra layers from explosive volcanism is commonly associated with the eruption of differentiated material (e.g. Fisher and Schmincke 1984), which is likely to contrast with the composition of proximal, generally less differentiated lavas. Petrogenetic models, however, are mostly built upon lavas, implying that tephra compositions cannot simply be taken as source area rock equivalents in petrogenetic studies. The problem of a compositional contrast is further enhanced, because phenocryst-bearing submarine tephra fallout layers are mostly characterized by their glass shard fraction, which is likely to differ from the bulk composition of the explosively erupted magma. Recently, temporally closely associated pyroclastic rocks and lavas from the same eruptive centre have been shown to reflect different primary magma compositions, with the tephra composition having been also strongly modified by crustal contamination (Freundt and Schmincke 1995). On the other hand, compositional contrasts between tephra and lavas might also reflect the composition of individual magma batches that evolved from a single parental melt in the course of fractional crystallization in crustal reservoirs.

In this study the glass fraction of vitric fallout tephra (<400 ka) deposited in the axial rift graben of the Mariana Trough spreading centre is investigated and the influence of shallow crustal differentiation on the composition of distal tephra fallout layers is discussed. Spatial and compositional arguments constrain the coeval subaerial and shallow submarine volcanoes of the Mariana arc to be the only sources. Despite a similar range in silica from basaltic to dacitic compositions, however, the glasses differ in having more enriched compositions and contrasting major element trends, implying a different petrogenesis for tephra and the Mariana arc volcanic rocks. A model is presented that establishes a genetic link between the contrasting compositions by complex fractional crystallization in crustal magma chambers.

Geological setting

Volcanism in the intraoceanic Mariana arc/backarc system is associated with the subduction of the Pacific plate beneath the Philippine plate in a westerly direction (Hussong and Uyeda 1981; Fig. 1). Since the initiation of subduction in the Eocene (≈40 Ma), the volcanic arc was twice split when backarc basins formed (≈32 Ma and ≈8–5 Ma) (e.g. Crawford et al. 1981; Natland and Tarney 1981). The present arc/backarc setting comprises from E to W (Karig 1971): (a) Mariana Trench; (b) Mariana Forearc; (c) Mariana volcanic arc; (d) Mariana Trough; and (e) West Mariana Ridge, an extinct remnant arc.

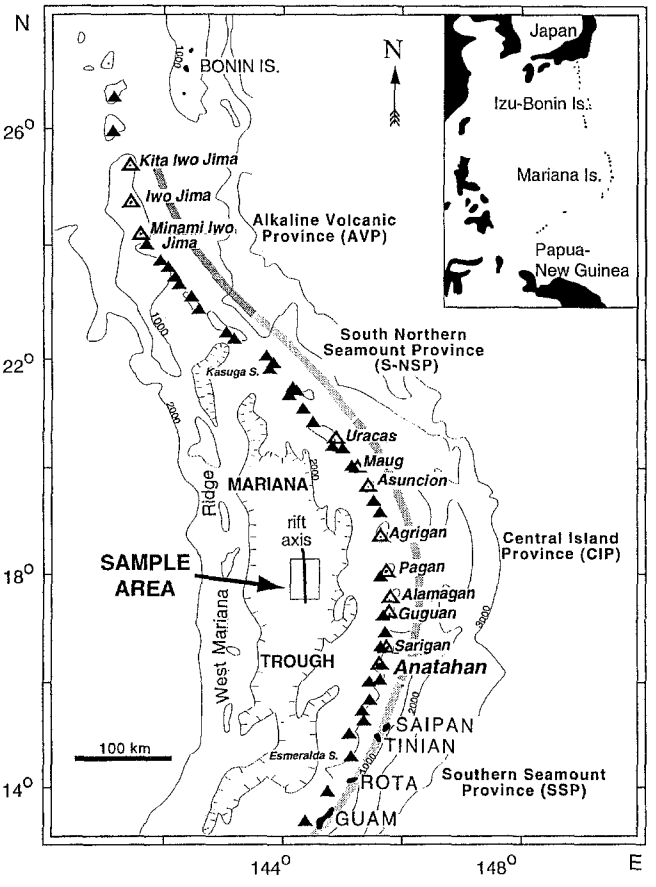

Fig. 1 Regional setting ofMarina arc/backarc system with subdivisions into provinces from Bloomer et al. (1989a). *Filled triangles* denote seamount volcanoes; *open triangles* subaerial volcanoes. Islands of frontal arc are indicated by capital letters. The sample area at the axial rift zone of the Mariana Trough is enlarged in Fig. 2

The crescent-shaped Mariana volcanic arc is active since at least 5 Ma (Packham and Williams 1981). It comprises nine subaerial and more than 30 submarine volcanic edifices (Bloomer et al. 1989a) that are built entirely on oceanic crust, which consists of young backarc crust (≈3–5 Ma) and older forearc crust (<45 Ma). The arc basement is estimated to be about 23 km thick (Sager 1980) and is composed mainly of tholeiitic and calcalkaline basalts to andesites and lavas similar to boninites, which are interspersed with subordinate dacites and rhyolites as well as calcareous and volcanigenic sediments (e.g. Schmidt 1957; Meijer 1980; Meijer and Reagan 1981; Wood et al. 1981; Reagan and Meijer 1984). Based on the spatial distribution of subaerial and submarine volcanoes and compositional characteristics, the arc is subdivided into four provinces (e.g. Bloomer et al. 1989a; Fig. 1). The Central Island Province (CIP) comprises the oldest and largest volcanoes. It extends towards the north and the south into chains of active seamount volcanoes named Northern Seamount Province (NSP) and Southern Seamount Province (SSP). The northernmost NSP (N-NSP) merges with the southernmost part of the Izu-Bonin arc between 22°

and 24°N. This part is also named Alkaline Volcanic Province (AVP) due to the occurrence of high-K, shoshonitic lavas (e.g. Stern et al. 1989; Bloomer et al. 1989a, b).

Mariana arc volcanoes erupt basalts through dacites with basaltic andesitic compositions being dominant. The occurrence of alkaline rocks is confined to the AVP; all other provinces have subalkaline compositions. Isotopic and trace-element data indicate enriched magma sources for the AVP and some S-NSP volcanoes (Meijer and Reagan 1983; Bloomer et al. 1989b; Lin et al. 1989), in contrast to the central and southern parts of the Mariana arc, which are less enriched and compositionally more uniform. Parental magma compositions of individual volcanoes within the central and southern Mariana arc, however, vary slightly due to small variations in degree of partial melting (Meijer and Reagan 1983) or slightly varying source compositions (e.g. Dixon and Stern 1983; Stern and Bibee 1984; Stern et al. 1989; Lin et al. 1989).

The seafloor of the Mariana Trough, an actively spreading backarc basin, has an average water depth of 4000 mbsl, with a central spreading ridge rising up to 3000 mbsl. The ridge is strongly segmented by along-strike normal faulting and perpendicular, E–W trending, transform-like offsets (e.g. Hawkins et al. 1990), and has a well-developed axial graben descending locally more than 5000 mbsl. Volcanic rocks comprise subalkalic basalt and basaltic andesites with compositions transitional between MORB and Mariana arc volcanic rock (e.g. Hart et al. 1972; Fryer et al. 1981; Volpe et al. 1987; Hawkins et al. 1990; Stern et al. 1990). Within-basin explosive pyroclastic volcanism is unlikely due to the high hydrostatic pressure ($\approx$0.3–0.5 kbar), which suppresses significant vesiculation even at the elevated volatile concentrations of the Mariana Trough basalts (up 2.1 wt.% H_2O; Stolper and Newman 1994).

Sample locations and samples

During RV SONNE cruise SO 57 in 1988, two box cores and one spade core were taken at 18°N in the Mariana Trough axial graben at 3860 to 4680 mbsl within a maximum distance of 25 km (Fig. 2; Table 1). The sites are located in a 60-km elongate depression within the axial graben that runs parallel to the rift axis

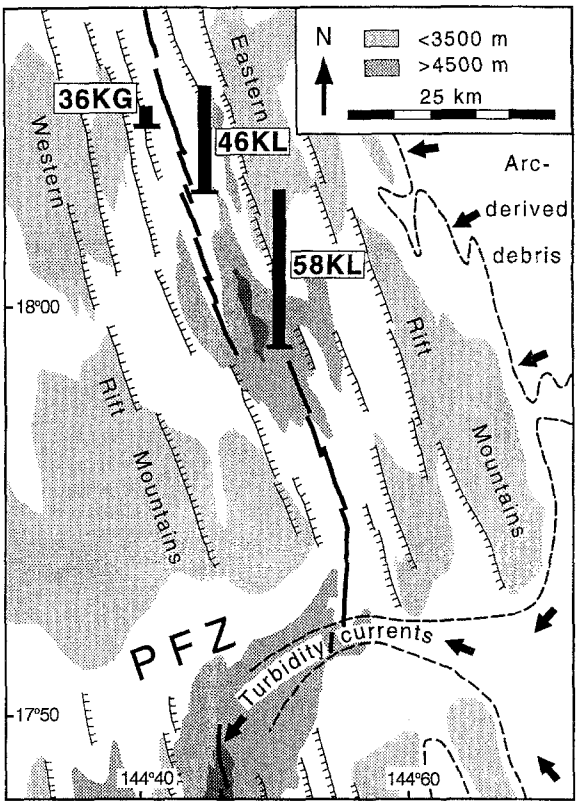

Fig. 2 Detail of the sample area in the axial rift zone of the Mariana Trough (modified from Hawkins et al. 1990). *Solid black line* marks active rift axis; *stippled line* shows the extent of arc-derived volcaniclastic mass flows. The sampling sites (spade core 37 KG; length 37 cm), box cores 46 KL (105 cm) and 58 KL (210 cm), are located in an elongate bowl-like depression within the axial graben, which is shielded from arc-derived mass flows by surrounding topographic highs. PFZ Pagan Fracture Zone

(Hawkins et al. 1990). Towards the S the axial graben floor rises to 4000 mbsl before it drops to 5000 mbsl in the E–W trending Pagan Fracture Zone. Thus, the sample area is effectively shielded from arc-derived volcaniclastic mass flows that cover the eastern half of the Mariana Trough and penetrate the Pagan Fracture Zone (Karig 1971; Bibee et al. 1980). Any arc-derived tephra in the sampling area must have been subaerially transported.

The axial graben seafloor is covered with a thin veneer of brown to grey-green, siliceous, carbonate-free clayey silts that are interspersed with layers of dark

Table 1 Locations of sediment cores and amount of samples investigated

Core no.	Position (Longitude/Latitude)	Water depth (m)	Core length (cm)	Discrete tephra layers	Surface samples[a]	Sediment samples[a]
36 KG	18°10.58N/144°41.48E	4090	37	3	1	—
46 KL	18°02.65N/144°46.83E	4700	105	12	1	2
58 KL	17°56.14N/144°50.31E	4680	225	13	1	—

In the text samples are identified by numbers: The first two digits give the core number and the others the depth in cm below the seafloor; thus, 3622 is the sample in 22 cm depth in core 36 KG

[a] Surface samples and sediment samples analyzed for dispersed glass shards

brown volcanic ash a few millimetres to a few centimetres thick. X-ray images of cores 36 KG, 46 KL and 58 KL (lengths from 37 to 225 cm) corroborated the presence of 3- to 10-mm thick primary tephra fallout layers. These show diagnostic sedimentary structures such as sharp bases, grain-size grading and either sharp or transitional tops. Each discrete tephra fallout layer that was not disturbed by bioturbation was sampled, resulting in a total of 28 fallout layers (Table 1). In addition, surface samples of all three cores were taken. A single 5-mm pumice lapillus was sampled in tephra fallout layer 5834. Two samples of clayey silt in core 46 KL at depths of 40 and 86 cm were analysed for dispersed glass shards. Most of the tephra sampled is fine sand-sized (70–150 μm average grain sizes) with only few particles exceeding several 100 μm in size.

The age of the cored sediment is roughly estimated around 400 ka, as inferred from the determination of the sedimentation rates by ^{230}Th in core 46 KL (analyst J. Scholten). This age is consistent with an estimated maximum age of about 400 ka of the newly formed seafloor in the axial graben, based on the assumption of symmetrical spreading, a spreading half rate of 15 mm/year (Bibee et al. 1980) and 12 km average width of the graben. The deposition of the tephra layers is thus contemporaneous to the subaerial MAV volcanic activity, which is estimated to cover approximately 1 Ma in age (Stern 1979; Meijer and Reagan 1981).

Mariana arc database

A total of 204 major element analyses (AVP: 20; S-NSP: 40; CIP: 119; SSP: 25; Mariana Trough Basalts: 130) were compiled from Hart et al. (1972), Larson et al. (1974), Dixon and Batiza (1979), Stern (1979), Meijer (1982), Meijer and Reagan (1981), Fryer et al. (1981), Dixon and Stern (1983), Stern and Bibee (1984), Volpe et al. (1987), Woodhead (1988, 1989), Bloomer et al. (1989b), Lin et al. (1989), Stern et al. (1989, 1990, 1993), Wolff (1990), Hawkins (1990) and Jackson (1989, 1993). About half of the samples were analysed for various compatible and incompatible trace elements, with the most comprehensive data sets given by Woodhead (1988, 1989) and Lin et al. (1989). Although pyroclastic rocks are reported to occur on all islands (e.g. Dixon and Batiza 1979; Stern 1979; Meijer 1982) and submarine arc volcanoes (Bloomer 1989a; Jackson 1993), few compositional data exist (e.g. Banks et al. 1984; Woodhead, *pers. commun.*), and to date no detailed study of pyroclastic material from the Mariana arc has been carried out. A detailed compositional comparison of subaerial and submarine tephra deposits is thus not possible. All compositional data were taken as published without any modification and without any assessment of interlaboratory bias, and thus are heterogeneous with regard to analytical methods and completeness of compiled trace-element data.

Analytical methods

Preparation

The tephra samples were shock-frozen, wet-sieved through a 35-μm screen of polyester gauze with distilled water and dried at 40 °C. From each sample about 30 glass shards with different morphologies and colours were handpicked under a binocular microscope, mounted and polished. The grain sizes of the handpicked glass shards ranges between 30 and 650 μm with the mean around 150 μm. Only fresh glass shards with crystal contents less than 30 vol.% were subjected to microprobe analysis.

Electron microprobe analysis

Electron microprobe analysis for ten major elements were performed by a CAMECA Camebax microprobe equipped with four spectrometers at the Mineralogical Institute of the University of Kiel. Natural and synthetic standards were used for calibration. Analyses were conducted with 15 kV accelerating voltage, a stationary, slightly defocussed beam (3 μm), 12 nA sample current and a counting time of 20 s for peak and 10 s for background measurements. Although Na and K were always among the first elements analyses, loss in Na could not be avoided (see caption of Table 2 for correction procedures). Although the sum of elemental oxides was only around 95 wt.% (Table 2), the sums were not normalized to a total of 100 wt.%, because the ef-

Table 2 Major element concentrations of glass shards exemplified by selected glasses from tephra layer 4646. b basalt; ba basaltic andesite; a andesite; d dacite; n. d. not determined

Shard no.	G33	g7	f6	D30	D30	p16	B28	c3
	b	b	ba	ba	ba	a	d	d
SiO_2[a]	50.4	51.6	54.2	56.1	56.1	61.3	63.4	64.2
TiO_2	1.3	1.3	1.3	1.3	1.3	0.7	0.4	0.6
Al_2O_3	12.7	14.8	14.6	14.1	14.1	14.4	15.5	14.9
FeO*	12.0	10.3	9.9	9.3	9.3	5.6	5.4	5.3
MnO	0.27	0.26	0.19	0.23	0.23	n. d.	0.12	0.17
MgO	4.9	3.2	2.7	2.1	2.1	1.3	1.5	1.2
CaO	9.7	8.1	6.9	5.9	5.9	4.1	4.5	3.4
Na_2O	2.8	2.9	3.3	2.9	2.9	3.1	2.6	3.0
K_2O	1.3	1.6	1.9	2.3	2.3	2.8	2.2	3.2
P_2O_5	0.34	0.35	0.46	0.53	0.53	n. d.	0.21	0.25
Total	95.8	94.4	95.4	94.8	94.8	93.3	95.8	96.2

Analytical precision and accuracy were monitored by alkaline and subalkaline dacitic glasses (alkaline glass SiO_2 = 64.6 wt.%; K_2O = 5.2 wt.%; Na_2O = 5.5 wt.%; subalkaline glass SiO_2 = 65.4 wt.%; K_2O = 0.6 wt.%; Na_2O = 2.74 wt.%). Measured Na_2O and K_2O were corrected by linear methods using concurrently analyzed Na_2O and K_2O concentrations of both reference glasses; measured SiO_2 was normalized to the silica content of the alkaline glass. Corrected centratons of repeated analyses agreed within the analytical error

[a] Oxides in wt.% with all Fe reported as FeO

fects of primary volatiles concentration and analytical problems (i.e. volatization) were considered to override variations that might be caused by secondary hydration. This is a reasonable assumption, because (a) any visual effects in brown glass shards were detectable, which are typical for the hydration of brown glass shards of basaltic through andesitic compositions (e.g. Fisher and Schmincke 1984), (b) tight elemental trends against an index of differentiation within individual ash layers give no indication of alteration-induced scattering, and (c) the primary volatile content of the glasses is unknown. Although the solubility of water at atmospheric pressure is basically zero, complex eruption dynamics (e.g. interaction with external water at deeper level of the conduit (Dunbar and Kyle 1992)) can partially suppress degassing in subaerial eruptions. Unpublished Fourier transform infrared spectroscopy (FTIR) results of vesicle-bearing, pristine brown glass shards of basaltic to andesitic composition glasses from several fallout tephra layers from the Izu-Bonin arc yield water contents in the range from 1–2 wt.% H_2O (Straub and Schmincke, in preparation). Major element concentrations of these shards are identical to melt inclusion compositions and give no indication of hydration-induced scattering. In summary, the primary volatile content cannot be assigned to be zero beforehand, and without definite proof for secondary hydration, the rise in silica content of several wt.%, which results from normalization, is not justified.

ICP-MS analysis

Glass shards from the compositionally least heterogeneous basaltic–andesitic layers (samples 3622, 5888 and 5894 with a less than 6 wt.% range in SiO_2) and the dacitic lapillus (tephra layer 5834) were selected for trace-element analysis (Table 3). Centrifuge-assisted gravitational separation based on sodium polytungstate solution (density of solution from 2.50 to 2.65 g/cm^3) was used to concentrate the basaltic–andesitic glass shards. The pumice lapillus was crushed in an agate mortar. All samples were separated from remnant phenocrysts and lithics by handpicking under a binocular microscope. The remaining glass fraction was rinsed repeatedly with distilled water. Trace-element analyses for 14 rare earth and 18 other trace elements were performed using a VG PlasmaQuad PQ 1 ICP mass spectrometer equipped with a VG multichannel analyser at the Geological Institute of the University of Kiel (analyst C. D. Garbe-Schönberg). Samples were not pulverized prior to analysis, but the small grain size and the vesicular structure provided large surficial areas for chemical attack and all solutions were clear and without visible remains. Samples were decomposed by pressurized HF-$HClO_4$-aqua regia attack. Details of the procedure as well as accuracy and precision are given in Garbe-Schönberg (1993).

Results

Glass shard characterization

The tephra layers investigated are composed of 80–100 vol.% volcanigenic particles and silicic bioclasts. Volcanigenic particles comprise green, brown and colourless glass shards (50–80 vol%), tachylites (up to 20%), volcanic lithic fragments (up to 10%) and phenocrysts (10–15 vol%). Phenocrysts consist of subequal portions of plagioclase and clinopyroxene in addition to subordinate titanomagnetite and rare orthopyroxene. The glasses are pristine with rare visible effects of alteration such as palagonitization or smectites. The shard morphologies comprise a wide range of dense, blocky, vesicle-bearing up to bubble-wall and highly vesicular shards, and indicate subaerial and shallow subaqueous explosive eruptions (e.g. Fisher and Schmincke 1984). A few layers contain shards with twisted droplet forms, which typically form during subaerial transport of low-viscosity melt. Brown and green vesicle-bearing and bubble-wall shards are most common, with dense, vesicle-poor and highly vesicular pumiceous shards being subordinate.

Two thirds of the tephra layers contain a second, subordinate glass shard population consisting of dark green blocky, vesicle-free sideromelane shards with basaltic and basaltic–andesitic compositions. The composition of these shards is identical to the backarc basin lavas, and they are interpreted to have been spalled from glassy rims of submarine lava flows and became admixed to the tephra fallout layers (Straub 1991). This population is not considered further in this paper.

Major element trends

The glass shards have medium-K to high-K basaltic through dacitic compositions (SiO_2 = 48–71 wt.%; K_2O = 0.8–3.2 wt.%; Fig. 3). The distribution is bimodal with a dominant maximum at basaltic–andesitic compositions ($\approx$ 52–57 wt.% SiO_2; approximately 80% of the glasses) and a subordinate maximum at dacitic compositions ($\approx$ 63–65 wt.% SiO_2). Glass shard compositions from individual tephra layers are similarly zoned with all layers containing basaltic–andesitic glass shards. Dacitic glasses, which occur only in 23 of the 31 layers investigated, have commonly coarser grain sizes (i.e. fine-sand sized). Silt-sized ash layers have mostly basaltic–andesitic glasses.

The general pattern of elemental variation with decreasing MgO is a decrease in CaO (11.5–0.4 wt.%), which is paralleled by a increase in SiO_2 (range 48–70 wt.%) and K_2O (0.8–3.2 wt.%). Despite considerable scatter, Na_2O (1.8–6.1 wt.%) increases only slightly and Al_2O_3 (11.7–17.2 wt.%) is invariant with decreasing MgO. P_2O_5 (0.2–0.6 wt.%), TiO_2 (0.4–1.7 wt.%) and FeO* (3.9–14.0 wt.%) first increase and

Table 3 Major and trace-element compositions of basaltic–andesitic glass shards and dacitic lapillus

	3622 Basaltic–andesitic glass shard separates	5888	5894	5834B Dacite lapillus	BR This work	BR Reference values[b]
Major elements (wt.%)						
SiO_2	53.8	54.6	55.6	65.7		
TiO_2	1.2	1.2	1.2	0.8		
Al_2O_3	14.4	14.4	14.6	14.6		
FeO*	10.9	8.4	7.3	5.7		
MnO	0.23	0.24	0.23	0.16		
MgO	2.8	2.6	2.6	1.2		
CaO	7.0	6.7	6.5	3.6		
Na_2O	3.4	3.3	3.3	3.6		
K_2O	1.9	1.9	2.0	2.8		
P_2O_5	0.42	0.43	0.39	0.28		
Total	96.04	93.73	93.66	98.53		
Trace elements (ppm)						
Rb	36	34	34	51	46	45
Sr	292	292	299	222	1332	1264
Y	33	33	33	39	26	26
Zr	117	120	112	208	271	260
Nb	2.8	2.4	3.4	7.0	146	116
Cs	1.3	1.2	1.4	1.7	0.9	0.82
Ba	444	493	428	451	1044	998
Hf	3.2	3.4	3.3	5.5	5.7	5.8
Pb	8.7	7.8	7.2	6.6	4.4	4.5
Th	1.5	1.5	1.4	2.6	10.1	9.8
U	0.8	0.8	0.7	1.4	2.6	2.5
La	12.43	12.27	12.00	15.48	80.30	76.90
Ce	27.58	27.22	26.24	34.53	145.03	144.00
Pr	4.04	4.15	4.06	4.90	16.34	16.20
Nd	19.32	19.62	18.18	22.24	65.46	61.90
Sm	5.46	5.56	5.22	5.95	11.61	11.60
Eu	1.59	1.61	1.53	1.48	3.59	3.47
Gd	5.84	5.99	5.64	6.50	10.24	9.56
Tb	0.99	0.99	0.94	1.07	1.30	1.24
Dy	6.31	6.36	6.04	6.92	6.39	6.05
Ho	1.30	1.31	1.24	1.44	1.02	1.00
Er	3.83	3.86	3.65	4.31	2.64	2.50
Tm	0.57	0.55	0.55	0.64	0.29	0.29
Yb	3.85	3.76	3.68	4.31	1.77	1.77
Lu	0.55	0.56	0.54	0.64	0.23	0.24
Sc	29	28	29	17	22	21
Cr	9	13	10	1	358	345
Co	26	25	27	9	61	59
Ni	8	12	12	1	260	255
Cu	240	234	237	23	76	71

[a] Concurrent analysis of USGS standard BR (basalt)
[b] Reference values from Garbe-Schönberg (1993)

then decrease with decreasing MgO. TiO_2 and FeO* simultaneously reach maximum concentrations around 4 wt.% MgO ($\approx$52 wt.% SiO_2), whereas P_2O_5 culminates around 2 wt.% MgO ($\approx$57 wt.% SiO_2) (Figs. 4 and 10a).

Within many layers glass shard compositions plot like "pearls on a string" against an index of differentiation. Significant compositional scatter, however, occurs as well within individual tephra layers as between different tephra layers. Within tephra layers off-trend compositions are due mostly to lower K_2O concentrations of individual glass shards, which may be as much as several tenths of a weight percent K_2O at a given SiO_2 content. As K_2O is typically taken up in the course of seawater alteration (e.g. Fisher and Schmincke 1984), these lower K_2O concentrations must reflect primary compositional variations of the magma. Significant deviations between individual tephra layers are due to (a) lower K_2O compositions at basaltic–andesitic compositions ($K_2O \approx 1$ wt.% contrasted to $K_2O \approx 1.5$ wt.% at equal wt.% SiO_2), which occur in all surface layers and in layers 5834 and 5847; and (b) the lower P_2O_5 compositions (0.2–0.3 wt.%) of basaltic–andesitic glass shards of tephra layer 5831, in contrast to

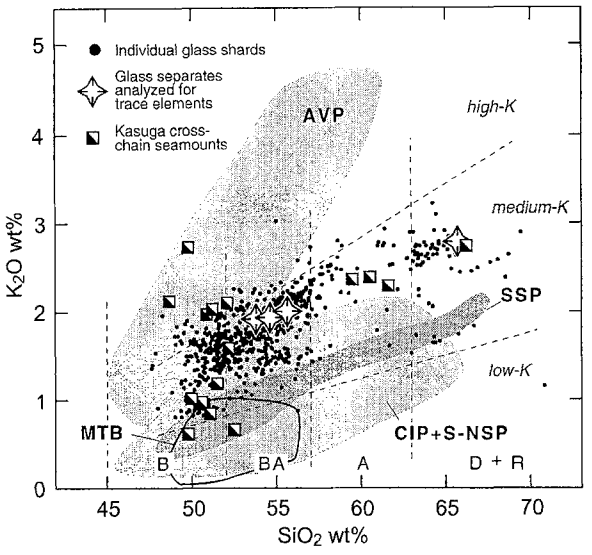

Fig. 3 K_2O-silica variation diagram illustrating the intermediate trend of glasses compared with Mariana arc volcanic rocks. *Stars* indicate bulk compositions of the basaltic–andesitic shards separates and the dacitic lapillus, which were analyzed for trace elements; *solid black line* encircles range of Mariana Trough basalts and basaltic andesites (MTB). Kasuga cross-chain seamounts are part of the S-NSP. Grid based on LeMaitre (1989). For Mariana arc/backarc data sources see text. AVP Alkaline Volcanic Province; CIP Central Island Province; S-NSP Southern Northern Seamount Province; SSP Southern Seamount Province (for location see Fig. 1)

≈ 0.5 wt.% P_2O_5 of the basaltic–andesitic glass shards of all other layers analysed. In addition, the layer 5831 basaltic–andesitic glass shards cluster tightly around ≈ 53 wt.% SiO_2 and ≈ 62 wt.% SiO_2 and do not form a continuous trend.

Trace elements

The trace-element concentrations of the three basaltic–andesitic glass separates are similar within analytical error. Incompatible trace elements of the dacitic pumice lapilli are on average 1.5 times more enriched than in the basaltic–andesitic glass shards, whereas transition elements (such as Sc, Cr, Ni, Cu and Zn) are 1–10 times depleted. Elemental enrichments and depletions are characteristic of subduction-related magma series (Fig. 5). Large-ion lithophile elements (LILE, such as K, Ba, Rb, Th and U) are enriched up to 100 times as compared with N-MORB, whereas Nb is depleted relative to other elements with a similar degree of mantle incompatibility (e.g. La/Nb$\approx$2–5; N-MORB and OIB$\approx$<1). High-field-strength elements (HFSE) are only slightly enriched (about 5 times on average). The glasses show typically high LILE/HFSE ratios such as Ba/La$\approx$35 (N-MORB and OIB<1); Ba/Zr$\approx$3.5 (N-MORB<0.1; OIB$\approx$1.25). The REE have 30–60 times chondritic concentrations and form smooth patterns with a small negative Eu anomaly (Eu/Eu*$\approx$0.8). The LREE are slightly enriched with $(Ce/Yb)_n$ ratios between 1.9 and 2.2.

Discussion

Compositional contrast between fallout tephra glasses and Mariana Arc volcanics.

Mariana arc volcanoes are the most likely sources for the investigated tephra layers due to (a) proximity, (b) temporal coincidence; (c) general similarity of major and trace element compositions and (d) matching source indicative trace-element ratios (Table 4; Fig. 6). A detailed comparison, however, shows that despite some overlap, the compositions of the glass shards are significantly different from Mariana arc volcanic rocks. Although both series range from basaltic to dacitic (Fig. 4), the K_2O concentrations of the glasses are intermediate between the low- to medium-K trend of the majority of the Mariana arc volcanoes and the shoshonitic trend of the AVP. Only the high-K trend of the Kasuga rear arc seamounts in the S-NSP overlaps in part with the glass shard compositions (Fig. 3).

The high K_2O concentrations of the AVP rules it out as source, as only few siliceous rocks (>55 wt.% SiO_2) have minor quantities of K-fractionating biotite (Bloomer et al. 1989b). Vitric tephra from such sources, however, would be relatively enriched in K_2O, and not depleted. In addition, distinct incompatible trace-element ratios (such as LREE/HREE and LILE/HFSE ratios; Table 4; Fig. 6) emphasize differences with the AVP. Based on incompatible trace-element ratios (e.g. $(Ce/Yb)_n$), some of the S-NSP volcanic centres, including the Kasuga seamounts, can also be excluded as volcanic sources, because they have the high, AVP-typical LREE/HREE ratios despite their low- to medium-K_2O trends (Table 4; Fig. 6). Incompatible trace-element ratios of the fallout tephra glasses, however, are within the range of most of the low- to medium-K Mariana arc volcanoes. (This group comprises all CIP and SSP and some of the S-NSP volcanoes and is termed MAV; see also Fig. 6.) Due to the compositional similarity, all MAV could be potential volcanic sources, because fallout tephra may also originate from explosive submarine eruptions (e.g. Fisher and Schmincke 1984; Bednarz and Schmincke 1994). The subaerial volcanoes, however, are most likely the continuous contributors of fallout tephra to the Mariana Trough sediments.

Compared with the MAV, however, glass shards in the fallout tephra layers investigated (glasses for short) occupy a compositionally distinct field with enriched compositions. The glasses reach a maximum of only 6.0 wt.% MgO in contrast to 11.4 wt.% MgO in the MAV (Pagan Volcano; Meijer 1982). Even when the MAV with MgO exceeding 6 wt.% are omitted, the glasses still have lower average MgO, Al_2O_3 and CaO and higher average K_2O, TiO_2, FeO* and P_2O_5 (Fig. 4)

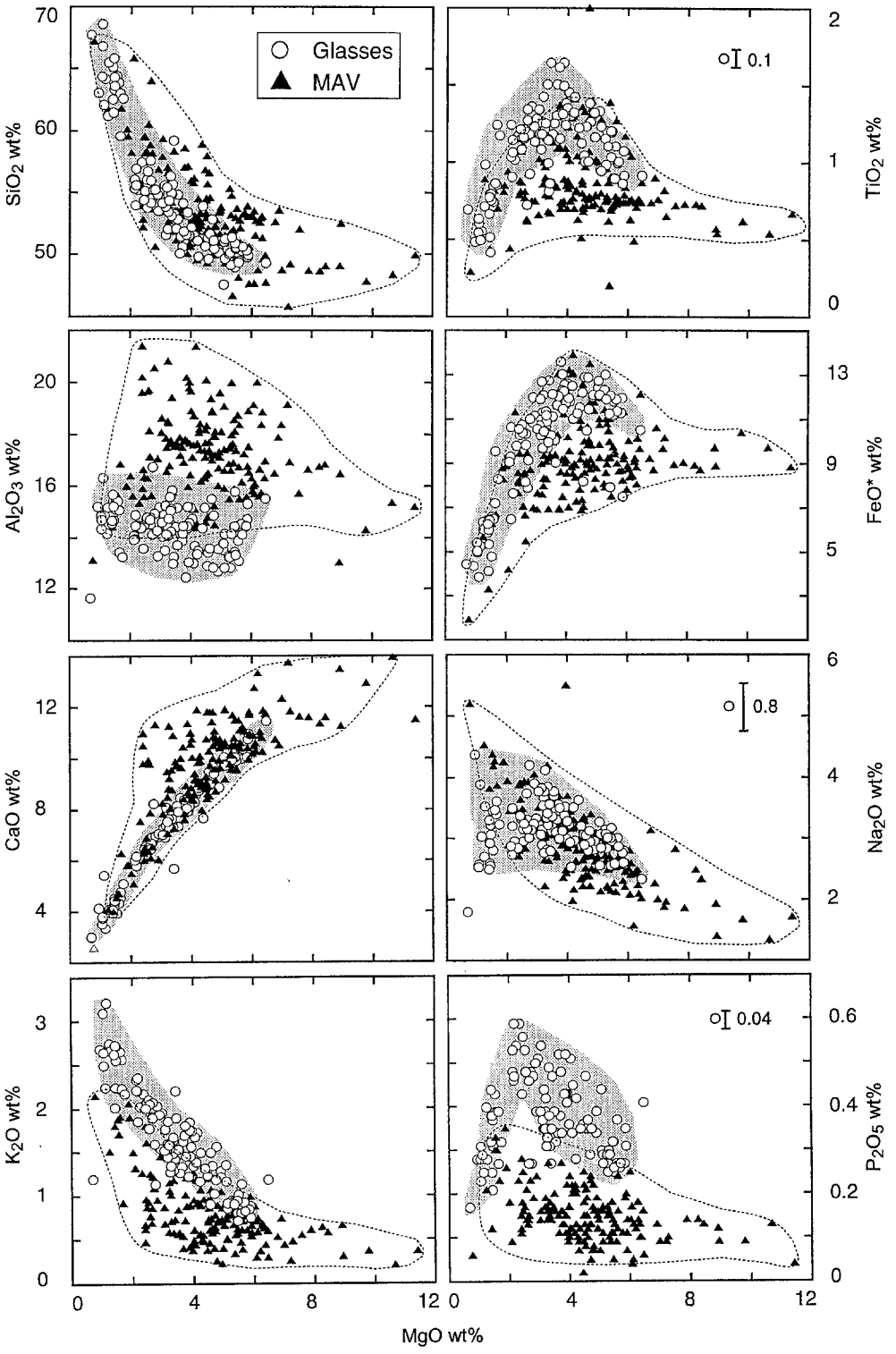

Fig. 4 Elemental variations of glass shards compared with Mariana arc volcanic rocks (MAV) compositions (see Fig. 6 for definition). Glass shard are selected compositions from eight fallout layers from three cores, all of which have basaltic trough dacitic compositions, and the three surface samples. Two sigma error for the glasses is within symbol size unless otherwise denoted. For Mariana arc/backarc data sources see text

than the lavas. In addition, the glasses are enriched in incompatible trace elements, with both the basaltic–andesitic and dacitic glasses being similar to the most enriched MAV (Fig. 5). Correspondingly, concentrations of the transition metals Sc, Ni, Co and Cr in the glasses are on the lower end of the MAV range.

The glasses represent the compositions of pure liquids that have already fractionated phenocrysts. Thus, when compared with bulk compositions of effusive rocks, exactly matching element concentrations cannot be expected. At first sight the compositional contrast between glasses and MAV seems to be derived from the fractionation of olivine, plagioclase, pyroxene and titanomagnetite, all minerals that are typical for the MAV. The increased FeO* and TiO_2 concentrations of the glasses could possibly be explained as a consequence of plagioclase-dominated crystallization in cooler, more differentiated regions of a magma chamber,

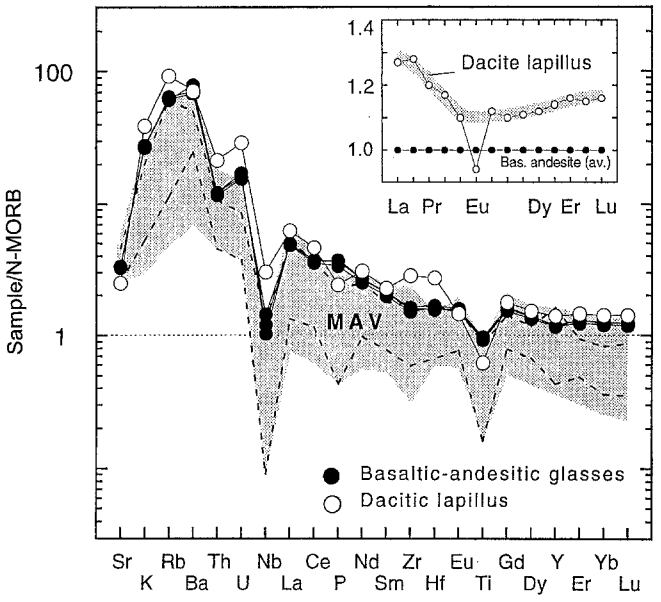

Fig. 5 Trace-element concentrations of glass shard and MAV compared with average N-MORB compositions [N-MORB compositions after Sun and McDonough (1989); elemental order based on Pearce (1983)]. *Shaded* maximum range of MAV trace-element variations; *broken lines* maximum range MAV basaltic andesites. Note small compositional range of basaltic–andesitic through dacitic glass shards and their overall enrichment. *Inset:* the slight relative MREE depletion of the dacitic lapillus compared with basaltic–andesitic glasses (average of three analyses) indicates apatite fractionation. The total mean REE enrichment (with the exception of plagioclase-controlled Eu) and the relative increase in LREE is attributed to the overruling effect of the combined precipitation of REE-refractory phases plagioclase, pyroxene and titanomagnetite, with the effect being further enhanced by comparatively low mean D_{apat}^{REE} at about 57 wt.% SiO_2 (probably below 10 according to experimental results of Watson and Green 1981)

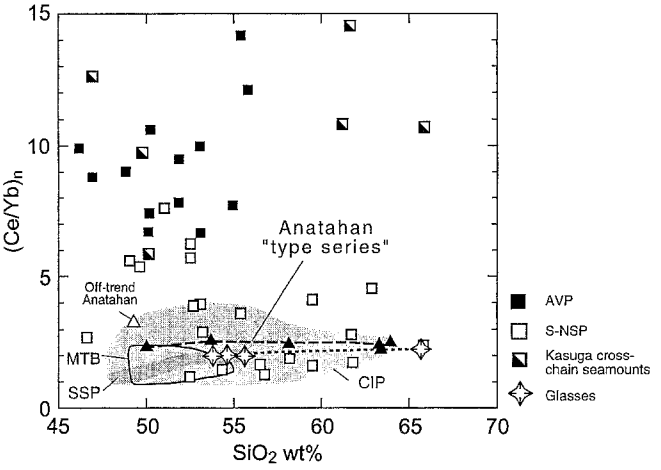

Fig. 6 Magma-source-indicative $(Ce/Yb)_n$ ratios rule out the AVP, the Kasuga cross-chain seamounts and some other of the S-NSP volcanoes as sources (see also Table 4). Volcanoes with $(Ce/Yb)_n$ ratios plotting in the shaded field, which is defined by all CIP compositions, are considered as potential sources and are termed Mariana arc volcanoes (MAV). $(Ce/Yb)_n$ ratios for the six samples of the Anatahan series $(Ce/Yb)_n \approx 1.9$)

similar to mechanisms that had been suggested to promote Fe and Ti enrichment in flank lavas of MOR (e.g. Bryan and Moore 1977).

If glasses and MAV major element *trends*, however, are compared, contrasting enrichment and depletion gradients appear, which cannot be explained by comparing porphyritic rocks to phenocryst-free compositions (Fig. 4). The contrasting trend is most striking for P_2O_5; the P_2O_5 trend of the glasses steeply increases until a maximum of 0.6 wt.% at $\approx$57 wt.% SiO_2 ($\approx$2 wt.% MgO), whilst the MAV lavas have a moderately increasing linear trend from 0.1% to 0.3 wt.% P_2O_5 with increasing SiO_2. The FeO* and TiO_2 contents of the glasses resemble those of the most enriched MAV, with the TiO_2 trend of the glasses culminating at slightly higher values than the MAV. The higher FeO* concentrations of the glasses, allied with lower MgO, result in higher FeO*/MgO ratios and thus in a distinct tholeiitic trend of fractionation. In contrast, the trend of the MAV is transitional between tholeiitic and calc-alkaline rocks (Fig. 7).

Common volcanic sources for the tephra layer glasses and the Mariana arc volcanics?

The enriched composition of the glasses may be explained by several models such as (a) origin from still-unknown MAV sources, (b) crustal contamination or (c) fractional crystallization. The existence of still-unknown volcanic sources in the MAV can be confidently ruled out, because the compositions of all Mariana arc volcanoes are well known with no "terra incognita" remaining. Even if such an enigmatic source existed, it would have to be the exclusive source of the tephra

Table 4 Incompatible trace-element ratios of basaltic–andesitic glasses compared with Mariana arc lavas with $SiO_2 < 57$ wt.%. AVP alkaline volcanic province

	Glasses ($n=3$)	MAV[a] ($n=62$)	Anatahan ($n=4$)	AVP ($n=13$)	Kasuga seamounts ($n=4$–10)
Rb/Zr	0.30± 0.01	0.20± 0.07	0.18± 0.03	0.69± 0.24	0.54± 0.34
Ba/Zr	3.9 ± 0.2	3.5 ± 1.1	3.7 ± 0.2	9.6 ± 4.8	3.1 ± 1.0
Ba/La	37 ± 3	38 ±11	35 ± 3	18 ± 3	17 ± 3
K/Rb	465 ±20	471 ±82	522 ±64	358 ±58	305 ±80
$(Ce/Yb)_n$	2.0 ± 0.02	2.3 ± 0.8	2.4 ± 0.1	9.3 ± 2.2	8.1 ± 2.0

[a] MAV all Mariana arc lavas with $(Ce/Yb)_n < 4$

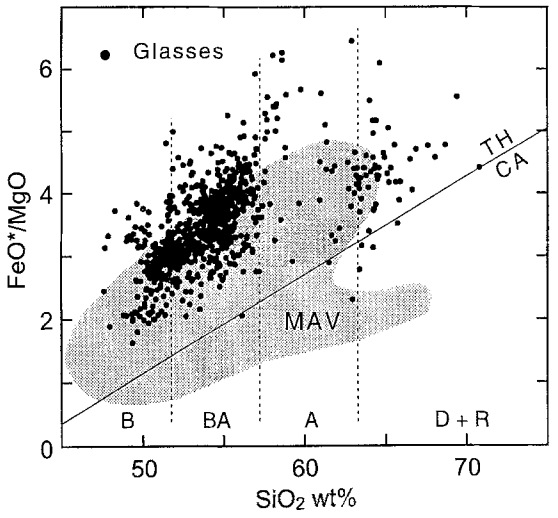

Fig. 7 Comparison of tholeiitic vs calc-alkaline fractionation trend of glasses and MAV. The majority of MAV volcanoes follows a tholeiitic trend of differentiation, whereas some small-volume volcanoes show transitional or dominantly calc-alkaline compositions (Meijer and Reagan 1981; Woodhead 1988; Jackson 1993). All compositions of glasses investigated with silica <57 wt.%, however, plot in the tholeiitic field. Dividing line from Miyashiro (1974)

layers. This condition, however, is incompatible with the fact that the central Mariana Trough is the major depositional site of the pyroclastic ejectas of *all* active arc volcanoes (Fig. 1), which have continuously erupted pyroclastic material during the period considered. Furthermore, crustal contamination is an unlikely cause for the enrichment of the glass shard melt. To date, studies of isotopic systematics in the Mariana arc, which include Sr, Nd, Th and O (e.g. Newman et al. 1984; Woodhead et al. 1987; Stern et al. 1993), give no evidence for significant contamination in the arc crust. In particular, the $\delta^{18}O$ values range between +5.7‰ and +6.6‰, and are indistinguishable from MORB (Stern and Bibee 1984; Woodhead et al. 1987; Stern et al. 1993). The ratios neither indicate any contamination with crustal volcanogenic sediment, as had been suggested as a cause for $\delta^{18}O$ enrichment in the Lesser Antilles island arc (e.g. Davidson 1985), nor remelting of hydrothermally altered crustal rocks, which lowers $\delta^{18}O$ (e.g. Marsh et al. 1991). Substantial contamination in oceanic volcanoes appears to occur in contact with an intrusive core consisting of evolved rocks (Freundt and Schmincke 1995). None of Mariana arc volcanoes, however, show evidence of having evolved intrusive rocks: All reported xenoliths are cumulate fragments of mafic and subordinate intermediate composition (e.g. Stern 1979; Woodhead 1988). None of them have a dominant K- or P-bearing phase, which could be a potential source of the K- and P-enrichment in the glasses.

On the other hand, compelling geochemical and petrographic evidence constrains fractional crystallization in high-level crustal reservoirs as the dominant cause of the compositional diversity of the Mariana arc volcanic rocks (Stern 1979; Dixon and Batiza 1979; Jackson 1993; Meijer and Reagan 1981; Woodhead 1988). In general, the most evolved dacitic compositions can be derived from basaltic parents by about 70% fractional crystallization (Stern 1979; Dixon and Batiza 1979; Woodhead 1988), although other mechanisms, such as magma mixing or gaseous transfer, have been suggested to have contributed to magma differentation (e.g. Stern 1979; Meijer and Reagan 1981; Jackson 1993). Several lines of evidence support an origin of the glass shard melt by fractional crystallization:

1. The composition of the most mafic glasses is clearly evolved in terms of indicators such as low maximum Mg # ≤53, Ni and Cr concentrations below 13 ppm as well as high FeO*/MgO ratios (≈2) in least-evolved compositions.
2. Mafic end members of glasses converge with MAV at higher MgO compositions, with some high-MgO glasses even having elemental concentrations similar to MAV compositions, suggestive of similar parental melts at higher MgO contents.
3. Incompatible trace-element enrichment is a typical consequence of fractional crystallization.

The different enrichment gradients and the separate elemental trends of glass shard and MAV melt, however, cannot originate by the same processes of fractional crystallization from common parental melts. I investigated the possibility that the emplacement of the marine tephra layers might highlight major, caldera-forming eruptions, which are associated with abundant pyroclastics of andesitic and dacitic composition (e.g. Stern 1979; Meijer and Reagan 1981; Meijer 1982). Stern (1979) observed on Agrigan that the lava compositions in the pre-caldera stage became progressively enriched in incompatible elements, until the most enriched andesites have absolute incompatible element contents that are similar to those of the glasses [e.g. Agrigan-Andesite: K_2O=2.1 wt.% (basaltic–andesitic glasses: 2.8 wt.%); P_2O_5=0.35 wt.% (0.41 wt.%); Zr=125 ppm (116 ppm); Rb=39 ppm (35 ppm)]. However, temporal constraints exclude such a correspondence, because the frequency of the marine fallout layers is much higher than the occurrence of climactic eruptions. On most of the islands only one caldera-forming eruption since emergence can be ascertained (on Agrigan, the oldest and largest of the subaerial volcanoes, the outline of a second older caldera is visible; Stern 1978), whereas the submarine MAV volcanoes have no caldera (Bloomer et al. 1989a). Considering the maximum subaerial lifetime of the island volcanoes of about 1 Ma (e.g. Meijer 1982), the frequency of caldera-forming eruptions can roughly be estimated at about one per 100 ka. In contrast, the tephra layer frequency averages about 30–40 ka, based on a sedimentation rate of about 19 mm/ka (Straub 1991). The eruption rates are probably even higher, because the host sediment also contains dispersed basaltic–andesitic glass shards with

the typically K_2O-, TiO_2- and P_2O_5-enriched compositions.

Discarding unknown volcanic sources and a relation to climactic eruptions provides some crucial constraints on the origin of the tephra layers. Firstly, and most obvious, the tephra layers must be derived from non climatic explosive eruptions of the MAV volcanoes, which continuously accompany their evolution. A good example for such an eruption is the 1981 Pagan plinian eruption, which produced an ash cloud that spread southward over most of the Mariana Trough area (Banks et al. 1984). Secondly, because the MAV volcanoes are the only available eruptive centres, glass shards and MAV melts must be generated in the same reservoirs. Thirdly, as it is highly unlikely that glass shard and MAV melts would originate from alternating eruptions that either tap glass shard or MAV melt batches from the same reservoirs, both melts must erupt simultaneously. Fourthly, the well-defined compositional contrast between glasses and MAV requires that two separate melts co-exist prior to eruption in a single reservoir. This implies that the MAV reservoir(s) must have been compositionally zoned, containing both the glass shard melt and the MAV melt. The remaining problem is: How did the glass shard melt and the MAV melt form in a single reservoir, and how did they physically separate prior to eruption?

Fractional crystallization link

Building on the assumption of common magma reservoirs and similar parental melts, I hypothesize that glasses and MAV melts might have been subjected to similar processes of fractional crystallization prior to the separation of their evolutionary trends, and that both series might have retained some common chemical signatures of this process. For this reason I have compared more closely the fractionation-induced multiple elemental variations of both MAV and glass shard melt compositions. Model calculations that were used to better constrain the variations of major and trace elements are given in the appendix.

Compositional variation of glass shards

Compositions of the dacitic glass shards can be derived from basaltic glasses by about 60–70% crystallization of a cumulate with average proportions of plagioclase and clinopyroxene (≈40–50 wt.%), orthopyroxene (≈3–4 wt.%), titanomagnetite (≈15 wt.%) and apatite (≈1 wt.%) (Table A1a). No olivine is required as it is consistent with the low maximum MgO of the glasses. Although qualitative trace-element variations are consistent with fractional crystallization, neither the Rayleigh fractionation equation nor the in situ equation can quantitatively reproduce the variation of the incompatible elements. The Rayleigh fractionation yields up to 20% higher mean increase of REE from basaltic–andesitic glasses to the dacite lapillus than observed. The in situ equation reproduces the results only at f values of about 0.4–0.6, i.e. if about half of the interstitial liquid in a marginal mush was extracted. Such an amount would require a mush of very low crystallinity (less than 50% crystal content) and a low-viscosity interstitial melt (at least basaltic), both conditions being incompatible with a dacitic derivative liquid.

The P_2O_5 decrease from andesitic to dacitic compositions (P_2O_5 drops from ≈0.5–0.6 to 0.2–0.3 wt.%) requires a P-fractionating phase (Figs. 3 and 10a). Apatite is the most likely phase, because being a ubiquitous accessory trace phase in subalkaline volcanic rock series (e.g. Gill 1981), the saturation of which is unavoidable in andesitic and dacitic magmas at the SiO_2 and P_2O_5 concentrations of the glasses (e.g. Watson and Green 1981; Green and Watson 1982). Apatite saturation is corroborated by the diagnostic slightly concave downward REE pattern relative to the assumed parental basaltic–andesitic glasses (Fig. 5). Thus, the observed P and REE variations strongly suggest the presence of apatite in the glass shards melt, despite not being observed modally. Apatite, however, often forms minute crystals, which can easily be overseen in lava flows, and may be even more difficult to observe in distal submarine tephra fallout.

The MAV exemplified by Anatahan

A cogenetic series from a single volcanic centre was used as a "MAV-type series" in order to minimize the possibility that the chemical variations were caused by processes other than fractional crystallization. The search for a "MAV-type volcano", however, was seriously restricted by the availability, completeness and quality of the up-to-now available major and trace-element data. Screening of the published data indicated Anatahan volcano as the presently best MAV counterpart because it has (a) a continuous basaltic to dacitic series; (b) high-quality major and trace-element data, including REE (Woodhead and Fraser 1985; Woodhead 1988, 1989); and (c) source-indicative trace-element ratios similar to those of the glasses (Fig. 6; Table 4).

Major and trace-element variations of six of the nine randomly sampled (Woodhead, *pers. commun.*) medium-K basalts to dacites (AN3-basalt, AN5-basaltic andesite, AN6-andesite, and three dacites AN12, AN10 and AN4; Figs. 5–7, 9 and 10) are diagnostic of low-pressure fractional crystallization (e.g. negative Al_2O_3, CaO, MgO and positive Na_2O, K_2O and P_2O_5 slopes with increasing silica, allied with invariant incompatible element ratios). Anatahan dacites can be modelled in three steps from Anatahan basalt AN3 by ≈70% crystallization of plagioclase, clinopyroxene, titanomagne-

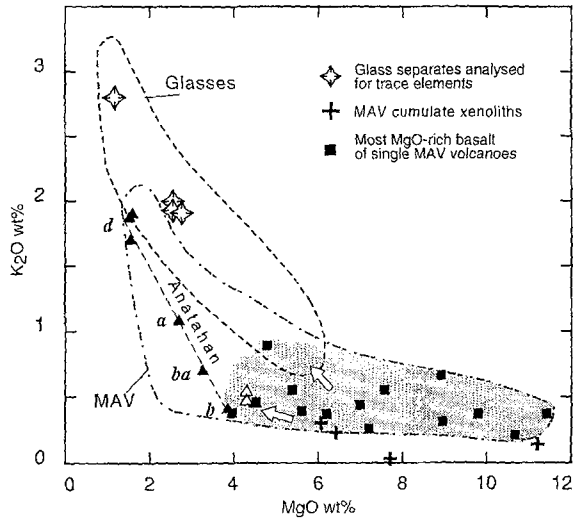

Fig. 8 K_2O vs MgO variation to illustrate the potential for common higher-MgO parental melts for glasses and MAV series. *Black squares* denote the most MgO-rich basaltic composition from individual MAV volcanic centres (only plotted if basaltic). Lower MgO compositions (<7 wt.% MgO) of MAV with the steeper K_2O gradient are considered to have evolved by fractional crystallization. Conspicuously, all glasses plot within this MgO range. The Anatahan basaltic to dacitic series (*black triangles*) is clearly differentiated with only 3.9 wt.% MgO for the basaltic end member AN3. *Open triangles* denote off-trend Anatahan compositions. b basalt; ba basaltic andesite; a andesite; d dacite

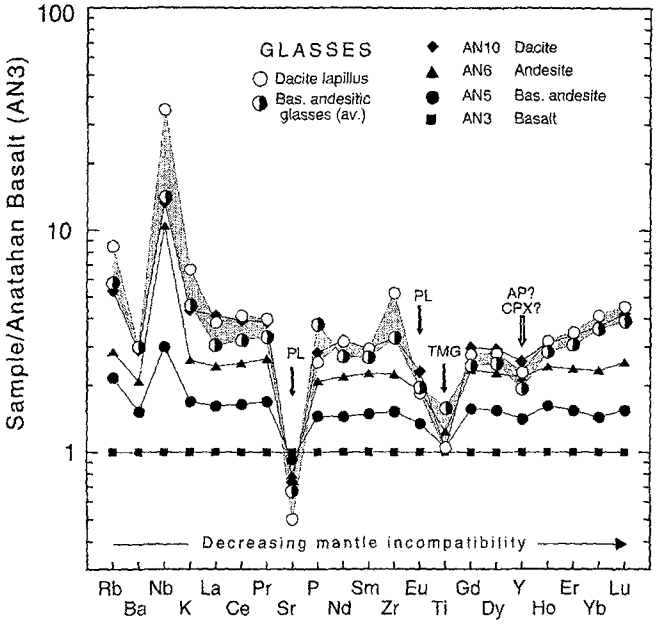

Fig. 9 Coryell-Matsuda diagram comparing fractionation-controlled (semi-)incompatible trace elements variation of Anatahan basalt though dacites to basaltic–andesitic through dacitic glasses [elemental ordering after Sun and McDonough (1981)]. All compositions are AN3 (basalt) normalized (Anatahan data from Woodhead 1989). For clarity, compositions of the three basaltic–andesitic glass shard separates are averaged. *Shaded:* total range of basaltic–andesitic to dacitic glasses. Note that the total variation of trace elements from basaltic–andesitic to dacite glasses comes to only about one fifth of the same silica range of the Anatahan series. *Arrows* indicate most prominent relative elemental depletions and the mineral host. Note higher contents of (semi-)incompatible elements P, Sr, Ti, Eu and possibly Ba in the less-differentiated basaltic–andesitic glasses compared with the dacite lapillus. The late-occurring Y depletion can either be attributed to clinopyroxene fractionation, because D^{Y}_{apat} increases with increasing silica from 0.5 to 4.0 from mafic to felsic compositions (Pearce and Norry 1979) or to incorporation into late-stage phase such as apatite ($D^{Y}_{apat} \approx 20$–40; Pearce and Norry 1979), the saturation of which is also suggested by the REE variations (Fig. 10). The Ba depletion relative to neighbouring Rb and Nb might in part reflect slightly increasing D^{Ba}_{plag} with increasing silica (0.23 to ≈1) (Arth 1976; Nash and Crecraft 1985). (PL plagioclase; CPX clinopyroxene; AP apatite; TMG titanomagnetite)

tite, olivine and orthopyroxene in the proportions of 63:20:9:5:3 that is typical for the MAV (e.g. Woodhead 1988; see also Table A1). The Rayleigh equation reproduces the increase in incompatible trace elements, except in the step from Anatahan andesite to dacite, where calculated concentrations are too low. A slighly higher degree of crystallization (about 20%) could amend this discrepancy. The excess enrichments in Anatahan dacite cannot be reproduced by the in situ equation at equal degrees of crystallization, even if the partition coefficients were assumed to be zero.

A puzzling problem in the evolution of the Anatahan dacites is the twofold relative MREE depletion that occurs at the transition from Anatahan andesites to dacites (Fig. 10b), because this signature cannot be caused by removal of an observed phase, but indicates the saturation of another, late-stage fractionating phase such as amphibole or apatite. However, amphibole can be ruled out as none of the Anatahan dacites contain amphibole; nor are amphibole-bearing cumulate fragments known from the MAV with the exception of Sarigan (Meijer and Reagan 1981). With D^{REE}_{amph}, which may be as high as 8–9 for the MREE in dacitic melts (Henderson 1982), about 5 wt.% of amphibole would be needed to cause the observed REE fractionation. With D^{Nb}_{amph} and D^{Zr}_{amph} being both 4 in dacitic liquids (Pearce and Norry 1979), this amount of amphibole would significantly deplete Zr and Nb in the residual melt, which is inconsistent with the observed increase of these elements (e.g. Fig. 9).

On the other hand, Anatahan dacitic melts should be close to or at apatite saturation with $P_2O = 0.3$ wt.% at the crustal pressures (≤7 kbar inferred from 25 km maximum crustal thickness) and temperatures (≈1000°T; Dixon and Batiza 1979; Meijer and Reagan 1981) of the Mariana arc magma chambers. At these temperatures and silica contents exceeding 60 wt.%, mean D^{REE}_{apat} range between 20 and 60 (Nagasawa 1970; Watson and Green 1981). Assuming mean D^{REE}_{apat} around 30–40, only trace amounts of apatite in the cumulate (≈0.5 wt.%) would be needed to cause the observed MREE depletion. Such a small amount of apatite can easily escape notice and, in addition, it also only buffers and not suppresses the overall P increase that is forced by the combined effect of the P_2O_5 refractory phases (e.g. Green and Watson 1982). Thus, de-

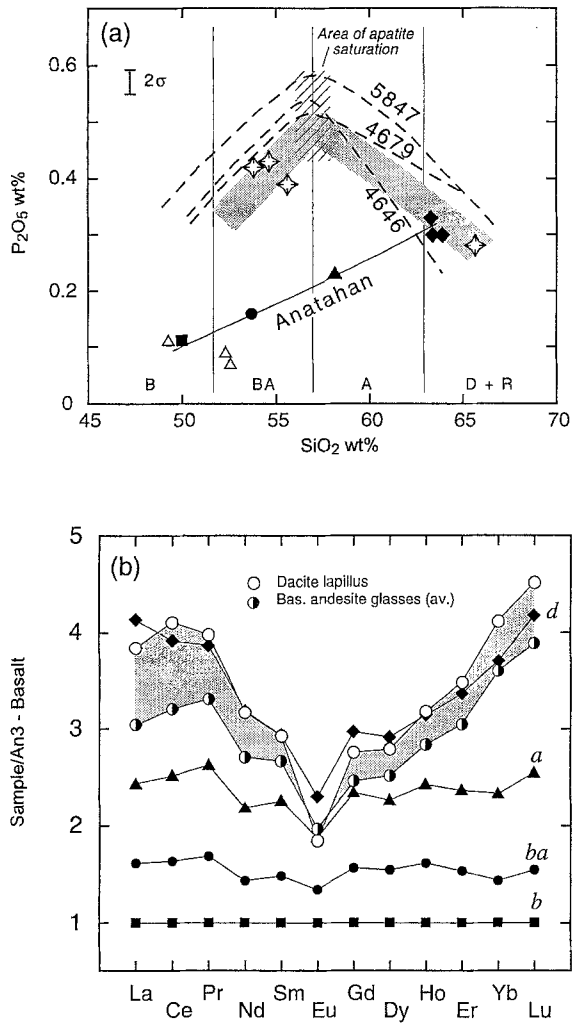

Fig. 10a, b The "apatite paradox" illustrated (see text for detailed discussion). **a** Inflections on individual trends of basaltic trough dacitic glasses of tephra layers 4646, 5831 and 5847 (*broken lines*) locate the area of apatite saturation (*hatched field*). *Stars:* Bulk compositions for glass shards separates and dacitic lapillus is analyzed for trace elements. *Thick-shaded line* highlights P_2O_5 trend for the glass shard separates as is inferred from P_2O_5 trends of glass shards from basaltic trough dacite layers. **b** Detail of the REE variation. Note that ordinate is not log-scaled in contrast to Fig. 9. b basalt; ba basaltic andesite; a andesite; d dacite. For other symbols see Fig. 9

spite apatite precipitation, the P_2O_5 trend may still increase.

In summary, modelling confirms that the chemical variation of both glass shards and the Anatahan series are controlled by fractional crystallization of similar mineral assemblages (with the exception of olivine). P and REE variations are consistent with late-stage apatite saturation in both series. The Rayleigh fractionation equation reproduces the incompatible trace-element variation better than the in situ equation, implying Rayleigh fractionation to be the dominant physical process for within series differentiation. Remaining discrepancies between modelled and observed incompatible element contents may well reflect the fact that neither the glasses nor the Anatahan samples are true parent–daughter pairs.

Comparison of fractionation patterns

In the following, the term *semi-incompatible* refers to elements that are generally considered as incompatible, but become compatible with regard to the fractionating mineral assemblage considered, e.g. Sr, Ti, Y and the REE. Due to the differing behaviour of incompatible and semi-incompatible elements during fractional crystallization, the Anatahan dacite is characterized by a multiple trace-element pattern, the pointed shape of which reflects the amount of the fractionating phases as well as the elemental partitioning behaviour (Fig. 9). Because these are intimately controlled by the physical and chemical conditions during fractional crystallization (e.g. temperature, pressure, kinetics of crystallization), the final shape of the pattern "fingerprints" the fractional crystallization process the Anatahan dacites have undergone. In Figs. 9 and 10b, the (semi-)incompatible trace-element variations of the glasses and the Anatahan series are shown relative to the assumed parental melt AN3. It is evident that the semi-incompatible element contents of both the *basaltic–andesitic and dacitic glasses* shards mimic the (semi-)incompatible trace element of the Anatahan *dacite*. Note that despite the lower degree of differentiation given by silica, the basaltic–andesitic glasses show an enrichment in (semi-)incompatible elements, which is comparable to the enrichment of the Anatahan dacite. The conformity of pattern of (semi-)incompatible elements of the glasses with the fractionation-induced pattern of the Anatahan dacite is considered as conclusive evidence that both series being intimately linked by fractional crystallization despite their contrasting major element trends.

Differentiation model

Figures 9 and 10 contain an important clue that helps to retrace the geochemical evolution of the glass shard melt: The P_2O_5 trends of the glasses in individual tephra layers indicate apatite saturation of the glass shard melt to occur around 57 wt.% SiO_2 and 0.5 wt.% P_2O_5 (Fig. 10a). Thus, basaltic–andesitic glasses at $\approx$54 wt.% SiO_2 and $\approx$0.4 wt.% P_2O_5 should not yet have reached apatite saturation. In Fig. 10b, however, the basaltic–andesitic glasses show the apatite-diagnostic MREE depletion. In other words, a melt that has not yet apatite on its liquidus shows its trace-element signature. How can that be?

Origin of glass shard fractionation pattern

The fractionated trace-element pattern of the glasses could be explained as mixture of a highly differentiated

– i.e. fractionated – melt and a larger amount of less-differentiated melt that were generated simultaneously by in situ crystallization from common parental melts in a single reservoir. In situ crystallization (=side-wall crystallization) refers to the faster crystallization of an initially homogenous magma body along a magma chamber wall due to the conductive loss of heat. In a strongly simplified view a compositionally "bi-polar" magma chamber forms with two different thermal and compositional regimes (e.g. McBirney 1980; McBirney et al. 1985): a cooler marginal zone characterized by a crystal-rich mush (crystal content ≈30–70%) that holds a highly differentiated interstitial liquid, and a hotter interior where the crystal content is low enough to be held in suspension by convection. This bi-polarity has two important consequences: (a) two strongly contrasting liquids can form in an early stage of the chamber evolution, – marginal interstitial liquid and liquid in the interior – without requiring large amounts of crystallization of the whole system or requiring different parental melts (Sparks et al. 1984); and (b) at the chamber margins the more extensive crystallization causes the saturation of phases that are not yet on the liquidus of the chamber interior (Langmuir 1989).

Evidence for in situ crystallization in MAV magma chambers is given from the pervasive occurrence of cumulate fragments, which may comprise as much as 15 vol.% in individual outcrops on the islands (e.g. Stern 1979; Meijer and Reagan 1981). The cumulate fragments, which are mostly gabbroic and composed by calcic plagioclase (70–80%) with subordinate olivine (0–24%) and clinopyroxene (0–3%), rare orthopyroxene and occasional titanomagnetite (up to 6 wt.%; Dixon and Batiza 1979; Stern 1979; Meijer and Reagan 1981; Woodhead 1988), have been interpreted by Stern (1979) to have resulted from in situ growth within, or just above, a liquid-crystal mush at the wall or the floor of a liquid reservoir. In a simplified, view a MAV magma chamber may be perceived as being subdivided into a liquid central part, dominated by liquids of basaltic to basaltic–andesitic MAV compositions, and a cooler marginal zone, where cumulate phenocrysts form a liquid-rich mush that has extractable liquid.

Any interstitial liquid of a mush dominated by typical MAV cumulate phenocrysts (i.e. plagioclase with subordinate olivine, pyroxene and oxides) would show the multiple chemical signatures of their fractionation. If this liquid were returned to the chamber interior, these characteristic signatures would became transmitted to the interior. A hybrid of returned and interior liquid would then show the chemical traces of the fractionation process at the chamber margin. A real MAV chamber interior, however, is unlikely to have remained wholly at an undifferentiated liquid stage, but could be perceived as a very low-concentrated suspension of ol±px±plag. In this case mixing with returned liquid would only enhance existing fractionation signatures. In other words, the chemical effect of the mixing process, which follows in situ crystallization, would be qualitatively indistinguishable from the chemical consequences of perfect fractional crystallization.

In the case of apatite, however, the matter is different. Apatite is very unlikely to be on the liquidus of a MAV chamber interior of basalt to basaltic–andesite compositions. Experimental work of Green and Watson (1982) has shown that at temperatures of 1000–1080 °C and $SiO_2 < 60$ wt.%, a minimum P_2O_5 of 0.7–1.0 wt.% is needed for apatite saturation. In view of the low P_2O_5 (0.2–0.3 wt.%) of MAV basalts and basaltic andesites even disequilibrium crystallization due to the sluggish diffusion of P and Si in front of advancing phenocryst surfaces (e.g. Green and Watson 1982; Bacon 1989) would cause apatite saturation concentration only at unrealistically high phenocryst growth rates ($\geqslant 10^{-9}$ cm/s). In contrast, apatite is very likely to precipitate in the mushy zone of the chamber margin, e.g. at $SiO_2 > 60$ wt.% (corresponds to about 50–70% crystallization) and at T < 1000 °C (e.g. 991 °C is given for a cumulate gabbro from Sarigan; Meijer and Reagan 1981). Apatite was indeed observed as intercumulus phases from Sarigan cumulates (Meijer and Reagan 1981). Thus, an interstitial liquid in an MAV marginal mush saturated in apatite would have low P_2O_5 (0.2–0.3 wt.%) and a relative MREE depletion. If this melt became mixed with a less differentiated chamber interior melt with initially low P_2O_5 (0.2 wt.%), the hybrid melt would be equally low in P_2O_5, but have a relative MREE depletion. Thus, in contrast to the depletion of the other semi-incompatible elements, the apatite signature, exemplified by the MREE depletion, is created by the in situ crystallization and serves as a chemical tracer of the process.

Tholeiitic trend of fractionation

In situ crystallization may also explain the tholeiitic trend of fractionation of the glasses (Fig. 7). During ideal in situ crystallization, the concentration of each element that is incompatible with regard to the mush is increased. Because the MAV mush is dominated by plagioclase with only subordinate Fe-Ti oxides (e.g. Stern 1979; Woodhead 1988), plagioclase-refractory elements Fe and Ti should become enriched in the interstitial liquid. With MgO being depleted in the glasses the FeO*/MgO ratio is increased resulting in a shift of glass compositions into the tholeiitic field. The tholeiitic trend of the glasses is then a consequence of fractional crystallization at crustal levels; it does not reflect the transitional and calc-alkaline trends that are both present in the MAV. In this case, magma-source-related processes, which may cause such trends as well (e.g. such a variable degree in mantle melting; Miller et al. 1992) cannot be inferred from the glass shard compositions.

Incompatible element enrichment

The newly mixed melt will be enriched in incompatible elements with the enrichment being dependent on the relative amounts of returned and interior liquid volumes. The hybrid melt must have basaltic compositions in order to be parental to the glass shards series. This implies that the amount of returned differentiated melt must be small compared with the more primitive interior melt, ranging between 1:9 and 1:8, when assuming silica concentrations of ≈ 62 wt.% SiO_2 (returned melt) and 47% SiO_2 wt.% (initial melt). At such ratios the concentrations of incompatible elements in the returned melt become strongly diluted and, despite some enrichment, the overall increase is far too small to account for the incompatible element contents of the glasses. This conclusion can be confirmed by using the in situ equation. Although a full set of trace-element compositions of basaltic glass shard compositions is not available, K_2O, one of most incompatible elements, can be used as an indicator for the increase in incompatible elements. Assuming an initial melt of 0.5 wt.% K_2O and 47 wt.% SiO_2 and a mean f of 0.5, the K_2O concentrations of the basaltic glass shards (≈ 1.2 wt.%) can only be achieved for an f value about 0.4, i.e. if more than half of the initial melt volume was crystallized. This mass cannot crystallize without a notable shift in major elements in the remaining liquid to more evolved compositions. Because the MAV magma chambers are clearly dominated by basaltic and basaltic–andesitic compositions, such a degree of crystallization can be ruled out. It follows that in situ crystallization alone cannot cause the total enrichment observed in the glass shards series, and additional mechanisms are needed to further enlarge the gap between incompatible and compatible (major) element concentrations of the glasses and the MAV melts.

Separation of glass shards melt

If the returned melt became fully mixed into the interior melt forming a single compositional regime, the two different fractionation series would never evolve. Thus, the basaltic liquid that is parental to the glasses must separate from the interior MAV magma. Physical processes of melt separation at this scale, however, cannot be resolved with the data at hand, and only a speculative approach to this problem can be made. I tentatively suggest that density-driven convective fractionation might provide a potential physical mechanism. Building on the results of fluid dynamic experiments McBirney (1980) and McBirney et al. (1985) discussed separation of melts of different densities that formed by side-wall crystallization. If the returned liquid is lighter than its surroundings, it forms a buoyant compositional boundary layer that flows up the wall and accumulates as a separate body in the upper level of the reservoir (Fig. 11). Experimental observations of the upstreaming flow

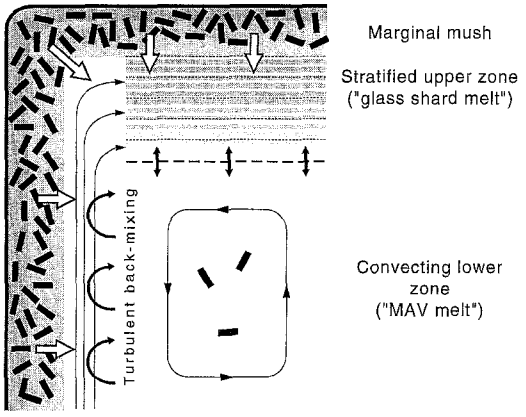

Fig. 11 Cartoon illustrating a model of generation, separation and co-existence of glass shard melt and MAV melt in a single magma chamber (modified from McBirney et al. 1985). Multiply-saturated (also apatite-saturated), fractionated interstitial melt of Si-andesitic to dacitic composition is returned from the mushy chamber margin (*white arrows*), where it buoyantly rises as marginal upstream (*thin black triple lines*) whilst entraining a larger portion of interior basaltic MAV melt ("backmixing", *crescent black arrows*). The hybrid melt is envisaged to accumulate as separate melt body at the chamber top, whereas the lower zone holds the MAV melts. Once separated, both zones evolve largely independently from each other. Note that the basaltic end member of the glasses is relatively enriched in FeO* and TiO_2 (see text for more details) and should therefore be slightly heavier (≈ 2.8 g/cm^3) than MAV basalts and basaltic–andesites (≈ 2.7 g/cm^3), causing it to sink instead to rise [anhydrous melt densities calculated after Bottinga et al. (1982) for T = 1000 °C and an arbitrary $FeO/Fe_2O_3 = 2$]. Such small density differences, however, could easily be offset if the hybrid melt was slighty enriched in water (less than 1 wt.% H_2O) and/or ferric iron relative to the interior melt (e.g. Bottinga and Weill 1970)

show it to be subdivided into two parallel zones: a thin laminar inner zone adjacent to the mush and a much wider turbulent zone in which less differentiated interior liquid becomes increasingly entrained in the upflowing stream (this process is termed "back-mixing" by McBirney et al. 1985). Such a process might account for the inferred condition of the returned melt becoming partially mixed with the interior melt.

Once the separation has taken place, the glass shard melt should occupy the upper zone of a MAV magma chamber, whereas the lower zone is occupied by the MAV melts (Fig. 11). In the analogue experiments of McBirney et al. (1985) the upper zone became stratified with regard to density with time by: (a) compositional change in upflowing liquids due to an increasing amount of backmixing with less differentiated interior liquid; (b) diffusive change through interface with the lower regime; and (c) input from differentiated melt from the roof region. These processes might further modify the glass shard melt composition, and also be responsible for the excess enrichment of the glasses as well as different enrichment gradients in incompatible elements (e.g. Nb compared with Zr or Rb; Fig. 9) in a way that cannot be assessed by the idealized models of Rayleigh fractionation and in situ crystallization.

Although speculative, a model using convective fractionation could explain two additional features. Firstly, it is obvious, that the compositional separation of such two intimately related series is not necessarily complete, and both series may have some compositions that are more akin to the other. This can easily explain the observed lower K_2O and P_2O_5 values of the glasses in some of the fallout tephra layers. Secondly, the correlation of eruptive style and the chemical compositions of the series could be explained. The enriched, strongly fractionated glass series are always associated with small-volume explosive eruption of the MAV, whereas the less-enriched MAV series is only represented by lavas. A likely cause for the explosive eruption of the glass shards melt is oversaturation by magmatic gases, that became preferentially enriched in the glass shards melt in contrast to the lower, less "processed" and more primitive MAV magma. The spatial separation of the two types of deposits (proximal lavas vs distal fallout), however, may be a sampling bias because proximal fallout tephra layers have not yet been studied and may show the same characteristics as the glasses investigated.

Conclusions

The following are conclusions of this work:

1. Vitric fallout tephra layers from Mariana arc explosive eruptions and lavas from the Mariana arc volcanoes form two compositionally contrasting series that evolved by fractional crystallization from similar parental magmas in shallow crustal magma chambers.
2. Detailed comparison of the fractionation patterns of (semi-)incompatible elements, rather than individual elemental variation, allows for constraining fractional crystallization as the genetic link between the series as well as for reconstructing the multi-stage fractionation process. The sub-liquidus signature of apatite – a late-stage crystallizing phase in these melts – in basaltic–andesitic glasses is considered as diagnostic of in situ crystallization.
3. Tephra studies are an important complement to Mariana arc petrogenetic models because they allow for more detailed models of magma-chamber processes in the Mariana arc than is possible from lavas.
4. Enrichment and differentiation trends of vitric fallout tephra reflect crustal differentiation in the Mariana arc and not magma-source-related processes. Thus, if glasses were uncritically taken as compositional equivalents of inaccessible or eroded source-area lavas, erroneous conclusions may result in studies addressing the long-term petrogenetic reconstructions of the Mariana arc evolution.

Acknowledgements I am indebted to C. W. Devey, A. Freundt, T. H. Hansteen, B. Köhler, D. Matthies and H.-U. Schmincke for long discussions and critical comments. Special thanks to J. Thiede for two years generous GEOMAR hospitality during this work. ICP-MS analyses were performed by C. D. Garbe-Schönberg (Geologisches Institut, Universität Kiel). J. Scholten determined the sedimentations rates of the core 46 KL by ^{230}Th methods. D. Ackermand and B. Mader are thanked for assistance with microprobe analyses. Laboratory work was assisted by W. Rehder and F. Werner. Financial support though the BMFT (Ministry for Research and Technology) of the Federal Republic of Germany is gratefully acknowledged. This paper benefitted from critical and thoughtful reviews by Shan de Silva and an anonymous reviewer.

Appendix

Model calculations

Major element trends were tested by mass balance using least-square methods of calculation. The results are tabulated in Table A1. The results given in Table A1 (b) and (c) were used for testing trace-element variations by assuming Rayleigh fractionation:

$$c_L = c_o \cdot F^{(D-1)}, \quad (1)$$

where c_L = element concentration in the daughter melt; c_o = element concentration in the parent melt, F = residual melt fraction, and D = bulk distribution coefficient given by $D = \Sigma D_a X_a$ with D_a = melt/mineral partition coefficient and X_a = amount of mineral fractionating.

Langmuir (1989) suggested an equation for the trace element variation by in situ crystallization:

$$c_L = c_o \cdot F^{[f\cdot(E-1)/(f-1)]}, \quad (2)$$

where F = residual melt fraction in the chamber interior after formation of a marginal crystal mush from an initially homogeneous magma body, f = melt fraction returned from marginal mush into the chamber interior; c_L = trace-element concentration in the chamber after mixing of re-injected liquid and liquid in the interior; $E = c_f/c_L$, where c_f = element concentration of residual melt in the mush. Assuming constant partition coefficients, E can be approximated as $E = [D\cdot(1-f)+f]^{-1}$.

Model calculations were confined to the REE, because all mineral compositions and melt/mineral partition coefficients were taken from the literature (see Table A2). This implies large uncertainties in addition to the fact that none of the compositions used are true parent–daughter liquids. Thus, instead of rigorously testing individual element variations, I tested whether the observed elemental variations are generally consistent with the fractionation mechanism proposed, or must be rejected.

Table A1 Selected results of mass balance calculations

Single glass shards within fallout tephra layer 4646							Glass shards separates and dacite lapillus analyzed for trace elements							Anatahan basalte to dacite						
Parent[a]	b		ba		a		Parent[a]	ba-3622		ba-5888		ba-5894		Parent[c]	AN3		AN5		AN6	
daughter	ba		a		d		daughter	d-5834		d-5834		d-5834		daughter	AN5		AN6		AN10B	
R	0.081		0.074		0.253		R	0.355		0.667		0.62		R	0.017		0.109		0.362	
F	0.625		0.855		0.773		F	0.608		0.658		0.682		F	0.679		0.664		0.744	
OLIV	–		–		–		OLIV	–		–		–		OLIV	7.43	*1*	6.93	*1*	–	
PLAG	27.48	*2*	54.35	*2*	29.65	*2*	PLAG	45.77	*2*	50.50	*2*	53.27	*2*	PLAG	69.00	*3*	72.94	*4*	47.99	*4*
CPX	62.62	*6*	34.04	*6*	36.74	*6*	CPX	32.27	*6*	33.74	*6*	34.57	*6*	CPX	18.22	*5*	15.10	*9*	27.64	*9*
OPX	–		–		–		OPX	–		–		–		OPX	–		–		8.17	*10*
TMG	9.90	*7*	11.61	*7*	29.90	*8*	TMG	20.28	*7*	14.01	*7*	10.93	*8*	TMG	5.55	*7*	5.53	*7*	16.02	*7*
AP	–		–		3.72		AP	1.69		1.75		1.23		AP	–		–		–	

Results in wt.%; R sum of squared residuals; F fraction of melt remaining. Sodium was omitted in all glass shard calculations
Compositions of mineral used are from Dixon and Batiza (1979); apatite is from Cox et al. (1979). *Italic* numbers behind the weight fraction of minerals refer to mineral code name as given in Dixon and Batiza (1979): *1* olivine GU3; *2* plagioclase P3; *3* plagioclase GU3; *4* plagioclase AG25; *5* clinopyroxene GU3; *6* clinopyroxene P3; *7* titanomagnetite P3; *8* titanomagnetite GU; *9* clinopyroxene AG25-1; *10* orthopyroxene Gu3b
[a] b basalt; ba basaltic andesite; a andesite; d dacite
[b] Each of the basaltic–andesitic glass shard separates was tested as potential parental to the dacite lapillus
[c] AN3 basalt; AN5 basaltic andesite; AN6 andesite; AN10B dacite

Table A2 Partition coefficients used in model calculations

Basaltic–andesitic to dacite glasses	La	Ce	Pr	Nd	Sm	Eu	Gd	Dy	Ho	Er	Yb	Lu	Reference
PLAG	0.14	0.14	0.11[c]	0.08	0.08	2.00	0.10	0.09	0.09[a]	0.08	0.07	0.08	Henderson (1982)
CPX	0.08	0.34	0.47[a]	0.60	0.90	0.90	0.85	1.10	1.05[a]	1.00	1.00	0.84	Henderson (1982)
OPX	0.02[b]	0.02	0.03[a]	0.05	0.05	0.05	0.04[a]	0.02	0.17[a]	0.31	0.34	0.11	Henderson (1982)
TMG	0.53	0.61	0.75[a]	0.88	0.93	0.58	0.9[a]	0.80	0.8[a]	0.8[a]	0.40	0.40	Henderson (1982)
AP	3.58	3.58	4.43	5.28	6.12	5.17	5.29	4.45	4.04	3.62	2.79	2.38	Watson and Green (1970)

Anatahan basalt to dacite[c]		La	Ce	Pr	Nd	Sm	Eu	Gd	Dy	Ho	Er	Yb	Lu	
OLIV	min	0[b]	0.009	0.008[a]	0.007	0.003	0.006	0.012	0.009	0.009[a]	0.009	0.009[b]	0.009[b]	Henderson (1982)
	max	–	–		0.010	0.015	0.010	–	0.014	–	0.017	–	–	
PLAG	min	0.1400	0.060	0.04[a]	0.020	0.020	0.320	0.030	0.010	0.01[a]	0.020	0.006	0.030	Henderson (1982)
	max	–	0.300	–	0.200	0.200	0.730	0.210	0.200		0.240	0.300	0.240	
CPX	min	0.0800	0.170	0.25[a]	0.320	0.320	0.480	0.820	0.560	0.55[a]	0.530	0.480	0.670	Henderson (1982)
	max	–	0.650	–	1.300	1.800	2.000	0.880	1.460	–	1.300	1.300	1.000	
OPX	min	0.003[b]	0.003	0.017[a]	0.030	0.010	0.020	0.070	0.120	0.140	0.160	0.110	0.110	Henderson (1982)
	max	–	0.040	–	0.060	0.100	0.080	–	0.290		0.460	0.670	–	
TMG	–	0.24	0.28	0.32	0.35	0.39	0.28	0.32	0.30	0.30	0.40	0.20	0.20	Henderson (1982)
AP	–	34.73	34.73	45.93[a]	57.13	62.8	30.45	56.76[a]	50.73	43.95[a]	37.18	23.85	20.25	Nagasawa (1970)

[a] Linear interpolated
[b] Assumed
[c] Partition coefficients were increased with increasing silica concentration of parent-daughter pair

References

Arculus RJ, Bloomfield AL (1992) Major-element chemistry of ashes from sites 782, 784, and 786 in the Bonin Forearc. In: Fryer P, Pearce JA, Stokking LB et al. (eds) Proc ODP Sci Results 125. College Station TX (Ocean Drilling Program) 125:277–292

Arth JG (1976) Behavior of trace elements during magmatic processes – a summary of theoretical models and their applications. J Res USGS 4:41–47

Bacon CR (1989) Crystallization of accessory phases in magma by local saturation adjacent to phenocrysts. Geochim Cosmochim Acta 53:1055–1066

Banks NG, Koyanagi RY, Sinton JM, Honma KT (1984) The eruption of Mount Pagan volcano, Mariana islands, 15 May 1981. J Volcanol Geotherm Res 22:225–269

Bednarz U, Schmincke HU (1994) Composition and origin of volcaniclastic sediments in the Lau Basin (SW-Pacific), ODP Leg 135 (sites 834–893). In: Hawkins J, Parson L, Allan J et al. (eds) Proc ODP Sci Results 135. College Station TX (Ocean Drilling Program) 135:51–74

Bibee LD, Shor GG, Lu RS (1980) Inter-arc spreading in the Mariana trough. Mar Geol 35:183–197

Bloomer SH, Stern RJ, Smoot NC (1989a) Physical volcanology of the submarine Mariana and Volcano arcs. Bull Volcanol 51:210–224

Bloomer SH, Stern RJ, Fisk E, Geschwind CH (1989b) Shoshonitic volcanism in the northern Mariana arc. J Geophys Res 94:4469–4496
Bottinga Y, Weill D (1970) Densities of liquid silicate systems calculated from partial molar volumes of oxide components. Am J Sci 269:169–182
Bottinga Y, Weill D, Richet P (1982) Density calculations for silicate liquids. I. Revised method for alumosilicate compositions. Geochim Cosmochim Acta 46:909–919
Bryan WB, Moore JG (1977) Compositional variations of young basalts in the Mid-Atlantic Ridge rift valley near lat 36°49′ N. Geol Soc Am Bull 88:556–570
Cox KG, Bell JD, Pankhurst RJ (1979) The interpretation of igneous rocks. Allan and Unwin, London
Crawford AJ, Beccaluva L, Serri G (1981) Tectono-magmatic evolution of the West Philippine-Mariana region and the origin of boninites. Earth Planet Sci Lett 54:346–356
Davidson J (1985) Mechanisms of contamination in Lesser Antilles island arc magmas from radiogenic and oxygen isotopes relationships. Earth Planet Sci 72:163–174
Dixon TH, Batiza R (1979) Petrology and chemistry of recent lavas in the northern Marianas: implications for the origin of island arc basalts. Contrib Mineral Petrol 70:167–181
Dixon TH, Stern RJ (1983) Petrology, geochemistry and isotopic composition of submarine volcanoes in the southern Mariana arc. Geol Soc Am Bull 94:1159–1172
Dunbar NW, Kyle PR (1992) Volatile contents of obsidian clasts in tephra from the Taupo volcanic zone, New Zealand: implications to eruptive processes. J Volcanol Geotherm Res 49:127–145
Fisher RV, Schmincke HU (1984) Pyroclastic rocks. Springer, Berlin Heidelberg New York
Freundt A, Schmincke HU (1995) Petrogenesis of rhyolite-trachyte-basalt composite ignimbrite P1, Gran Canaria, Canary Island. J Geophys Res 100 (B1):455–474
Fryer P, Sinton JM, Philpotts JA (1981) Basaltic glasses from the Mariana Trough. In: Hussong D, Uyeda S et al. (eds) Init Repts DSDP 60. Washington (US Govt Printing Office) 60:71–74
Garbe-Schönberg CD (1993) Simultaneous determination of thirty-seven trace elements in twenty-eight international rock standards by ICP-MS. Geostandards Newsletter 17 (1):81–97
Gill J (1981) Orogenic andesites and plate tectonics. Springer, Berlin Heidelberg New York
Green TH, Watson EB (1982) Crystallization of apatite in natural magmas under high pressure, hydrous conditions, with particular reference to orogenic rock series. Contrib Mineral Petrol 79:96–105
Hart SR, Glassley WE, Karig DE (1972) Basalts and sea floor spreading behind the Mariana island arc. Earth Planet 15:12–18
Hawkins JW, Lonsdale JD, Macdougall JD, Volpe AM (1990) Petrology of the axial ridge of the Mariana trough backarc spreading center. Earth Planet Sci Lett 100:226–250
Henderson P (1982) Inorganic geochemistry. Pergamon Press, London
Hiscott RN, Gill JB (1992) Major and trace element geochemistry of Oligocene to Quarternary volcaniclastic sands and sandstones from the Izu-Bonin arc. In: Taylor B, Fujioka K et al. (eds) Proc ODP Sci Results 126. College Station TX (Ocean Drilling Program) 126:467–485
Hussong DM, Uyeda S (1981) Tectonic processes and the history of the Mariana arc: a synthesis of the results of Deep Sea Drilling Project Leg 60. In: Hussong DM, Uyeda S et al. (eds) Init Repts DSDP 60. Washington (US Govt Printing Office) 60:909–929
Jackson MC (1989) Petrology and petrogensis of recent submarine volcanics from the northern the Mariana arc and backarc basin. Unpublished PhD Thesis University of Hawaii
Jackson MC (1993) Crystal accumulation and magma mixing in the petrogenesis to tholeiitic andesites from Fukujin Seamount, Northern Mariana Island Arc. J Petrol 34 (2):259–289
Karig DE (1971) Origin and development of marginal basins in the western Pacific. J Geophys Res 76:2542–2561
Langmuir CH (1989) Geochemical consequences of in situ crystallization. Nature 340:199–205
Larson EE, Reynolds RL, Merrill R, Levi S, Ozima M, Aoki Y, Kinoshita H, Zasshu S, Kawai N, Nakajima T, Hirooka K (1974) Major-element petrochemistry of some extrusive rocks from the volcanically active Mariana islands. Bull Volcanol 38:361–377
LeMaitre RW (ed) (1989) A Classification of Igneous Rocks. Blackwell Scientific Publications. Oxford London Edinburgh Boston Melbourne
Lin PN, Stern RJ, Bloomer SH (1989) Shoshonitic volcanism in the northern Mariana arc 2. Large-ion lithophile and rare earth element abundances: evidence for the source of incompatible element enrichments in intraoceanic arcs. J Geophys Res 94:4497–4514
Marsh BD, Gunnarson B, Congdon R, Carmody R (1991) Hawaiian basalt and Icelandic rhyolite: indicators of differentiation and partial melting. Geol Rundsch 80 (2):481–510
McBirney AR (1980) Mixing and unmixing of magmas. J Volcanol Geotherm Res 7:357–371
McBirney AR, Baker BH, Nilson RH (1985) Liquid fractionation. Part I: Basic principles and experimental simulations. J Volcanol Geotherm Res 24:1–24
Meijer A (1980) Primitive arc volcanism and a boninite series: examples from western Pacific island arcs. Geol Soc Am Bull 23:269–282
Meijer A (1982) Mariana volcano islands. In: Thorpe RS (ed) Andesites. John Wiley, pp 293–306
Meijer A, Reagan M (1981) Petrology and geochemistry of the island of Sarigan in the Mariana arc; calc-alkaline volcanism in an oceanic setting. Contrib Mineral Petrol 77:337–354
Meijer A, Reagan M (1983) Origin of K_2O-SiO_2 trends in volcanoes of the Mariana arc. Geology 11:67–71
Miller DM, Langmuir CH, Goldstein SL, Franks AL (1992) The importance of parental magma composition to calc-alkaline and tholeitic evolution: evidence from Ummak Island in the Aleutians. J Geophys Res 97 (B1):321–343
Miyashiro A (1974) Volcanic rock series in island arcs and active continental margins. Am J Sci 274:321–355
Nagasawa H (1970) Rare earth concentrations in zircons and apatites and their host dacites and granites. Earth Planet Sci Lett 9:359–364
Nash WP, Crecraft HR (1985) Partition coefficients for trace elements in silicic magmas. Geochim Cosmochim Acta 49:2309–2322
Natland JH, Tarney J (1981) Petrologic evolution of the Mariana arc and back-arc basin system – a synthesis of drilling results in the South Philippine Sea. In: Hussong D, Uyeda S et al. (eds) Init Repts DSDP 60. Washington (US Govt Printing Office) 60:877–908
Newman S, Macdougall JD, Finkel RC (1984) ^{230}Th-^{238}U disequilibrium in island arcs: evidence from the Aleutians and the Marianas. Nature 308:268–270
Packham GH, Williams KL (1981) Volcanic glasses from sediments from sites 453 and 454 in the Mariana Trough. In: Hussong D, Uyeda S et al. (eds) Init Repts DSDP 60. Washington (US Govt Printing Office) 60:483–497
Paterne M, Guichard F, Labeyrie J (1988) Explosive activity of the south Italian volcanoes during the past 80000 years as determined by marine tephrochronology. J Volcanol Geotherm Res 34:153–172
Pearce JA, Norry MJ (1979) Petrogenetic implications of Ti, Zr, Y and Nb variations in volcanic rocks. Contrib Mineral Petrol 69:33–47
Pearce JA (1983) Role of the sub-continental lithosphere in magma genesis at active continental margins. In: Hawkesworth CJ, Norry MJ (eds) Continental basalts and mantle xenolithes. Birkhäuser Boston Nantwich Shiva Cambridge pp 230–249

Reagan MK, Meijer A (1984) Geology and geochemistry of early arc-volcanic rocks from Guam. Geol Soc Am Bull 95:701–713

Sager WW (1980) Mariana arc structure inferred from gravity and seismic data. J Geophys Res 85:5382–5388

Schmidt RG (1957) Petrology of the volcanic rocks. In: Cloud PE et al. (eds) Geology of Saipan Mariana islands. US Government Printing Office (Geol Surv Prof Pap), Washington, part 2, chapter B, pp 127–172

Simon-Neuser M, Schmincke HU (in press) Cretaceous and Eocene volcanism at the paired aseismic ridges Walvis Ridge and Rio Grande Rise, South Atlantic. Mar Geol

Sparks RJS, Huppert HE, Turner JS (1984) The fluid dynamics of evolving magma chambers. Phil Trans R Soc Lond A 310:511–534

Stern RJ (1978) Agrigan: an introduction to the geology of an active volcano in the nothern Mariana island arc. Bull Volcanol 41:43–55

Stern RJ (1979) On the origin of andesite in the northern Mariana island arc: implications from Agrigan. Contrib Mineral Petrol 68:207–219

Stern RJ, Bibee LD (1984) Esmeralda Bank: geochemistry of an active submarine volcano in the Mariana island arc. Contrib Mineral Petrol 86:159–169

Stern RJ, Bloomer SH, Lin PN, Smoot NC (1989) Submarine arc volcanism in the southern Mariana arc as an ophiolite analogue. Tectonophysics 168:151–170

Stern RJ, Lin PN, Morris JD, Jackson MC, Fryer P, Bloomer SH, Ito E (1990) Enriched back-arc basin basalts from the northern Mariana Trough: implications for the magmatic evolution of back-arc basins. Earth Planet Sci Lett 100:210–225

Stern RJ, Jackson MC, Fryer P, Ito E (1993) O, Sr, Nd and Pb isotopic compositions of the Kasuga cross-chain in the Mariana Arc: a new perspective on the K-h-relationship. Earth Planet Sci Lett 119:459–475

Stolper E, Newman S (1994) The role of water in the petrogenesis of Mariana Trough magmas. Earth Planet Sci Lett 121:293–325

Straub SM (1991) Zusammensetzung und Herkunft mariner Aschelagen aus dem Marianen Backarc Trog. Unpublished PhD Thesis Universität Kiel

Sun SS, McDonough WF (1989) Chemical and isotopic systematics of oceanic basalts: implications for mantle composition and processes. In: Saunders AD, Norry MJ (eds) Magmatism in the ocean basins. Geol Soc Spec Publ, Blackwell, Oxford, pp 313–345

Volpe AM, Macdougall JD, Hawkins JW (1987) Mariana Trough basalts (MTB): trace element and Sr-Nd isotopic evidence for mixing between MORB-like and arc-like melts. Earth Planet Sci Lett 82:241–254

Watson EB, Green TH (1981) Apatite/liquid partition coefficients for the rare earth elements and strontium. Earth Planet Sci Lett 56:405–421

Wolff G (1990) Geochemische, petrographische und petrologische Untersuchungen an Vulkaniten des Marianen Beckens. Unpublished MSc Thesis. Universität Kiel

Wood DA, Marsh NG, Tarney J, Joron JL, Fryer P, Treuil M (1981) Geochemistry of igneous rocks recovered from a transect across the Mariana trough, arc, fore-arc, and trench, sites 453 through 461, Deep Sea Drilling Project Leg 60. In: Hussong DM, Uyeda S et al. (eds) Initial Rpts of DSDP 60. Washington (US Govt Printing Office) 60:611–646

Woodhead JD, Fraser DG (1985) Pb, Sr and ^{10}Be isotopic studies of volcanic rocks from the northern Mariana islands. Implications for magma genesis and crustal recycling in the western Pacific. Geochim Cosmochim Acta 49:1925–1930

Woodhead JD, Harmon RS, Fraser DG (1987) O, S, Sr and Pb isotope variations in volcanic rocks from the northern Mariana islands: implications for crustal recycling in intra-oceanic arcs. Earth Planet Sci Lett 83:39–52

Woodhead JD (1988) The origin of geochemical variations in Mariana lavas: a general model for petrogenesis in intra-oceanic island arcs? J Petrol 29:805–830

Woodhead JD (1989) Geochemistry of the Mariana arc (western Pacific): source composition and processes. Chem Geol 76:1–24